# Chapter 1

# Introduction

## 1.1 Aims and objectives

This thesis is focused on atomic modelling for diagnostic analysis of plasmas through observation of their spectra. It is recognised that spectroscopy of high temperature plasmas provides probably the most sensitive and revealing type of measurement which can be made on atoms. Such studies are applicable whether the plasma is remote as in astrophysics or nearby in the laboratory. The emitting atoms are in many circumstances revealing of the environment in which they lie and it is these situations which provide the diagnostic opportunities. Consider the solar chromospheric/coronal plasma and the laboratory fusion plasma. They have marked similarities from the point of view of spectral emission, although their energy input mechanisms are quite different. Both are high temperature plasmas with the solar upper atmosphere electron temperature ranging from $\sim 2 \times 10^4 K$ to $\sim 2 \times 10^6 K$ in the quiet sun and up to $\sim 1 \times 10^7 K$ in flares. The modern fusion plasma, such as the Joint European Torus (JET) tokamak, is of somewhat higher temperature at $\sim 3 \times 10^7 K$ to $\sim 2 \times 10^8 K$ ($3keV$ to $20keV$) in the core, but with temperatures in the key divertor plasma very similar to the solar case. The core fusion plasma has electron densities of $\sim 3 \times 10^{13} - 1 \times 10^{14} cm^{-3}$ while the solar coronal plasma is of lower density at $\sim 1 \times 10^8 cm^{-3}$ but rising steadily as one moves down through the chromosphere. Both types of plasma display marked gradients in temperature and density (compare

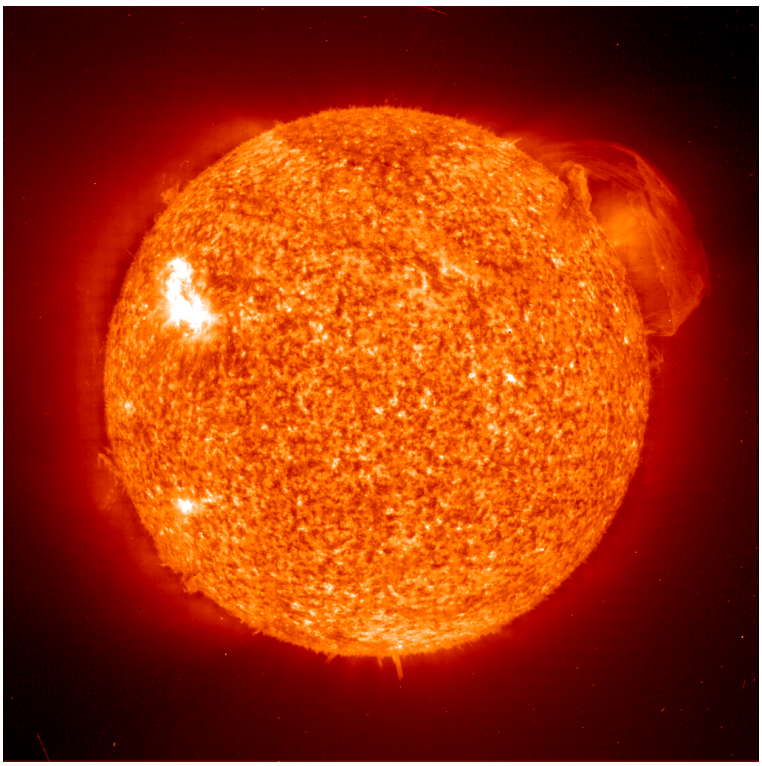

Figure 1.1: He 304 Å observation of the solar chromosphere at $T_e \sim 40,000K$, taken using the EIT instrument onboard the SOHO spacecraft.

the solar transition region and high shear layers and H-mode pedestals in the fusion case) quite apart from local disturbances and instabilities. These temperatures ensure that the plasma is highly ionised and the relatively low densities mean that the ion environment is far from local thermodynamic equilibrium. Also, the dimensions of the plasmas ensure that one has in general easy escape, that is optical thinness, of the emitted radiation. For these reasons, the spectral analysis for these two types of plasma has developed similarly in a modelling picture which even in the fusion case is often called 'coronal'.

With the development of X-ray telescopes and new satellites and spacecraft with scientific payloads (e.g. the Hubble Space Telescope, SOHO, TRACE, CHANDRA) there are few spectral regions left that cannot be measured. This means that the spectra resulting from almost any possible atomic transition can be observed and diagnostic information obtained.

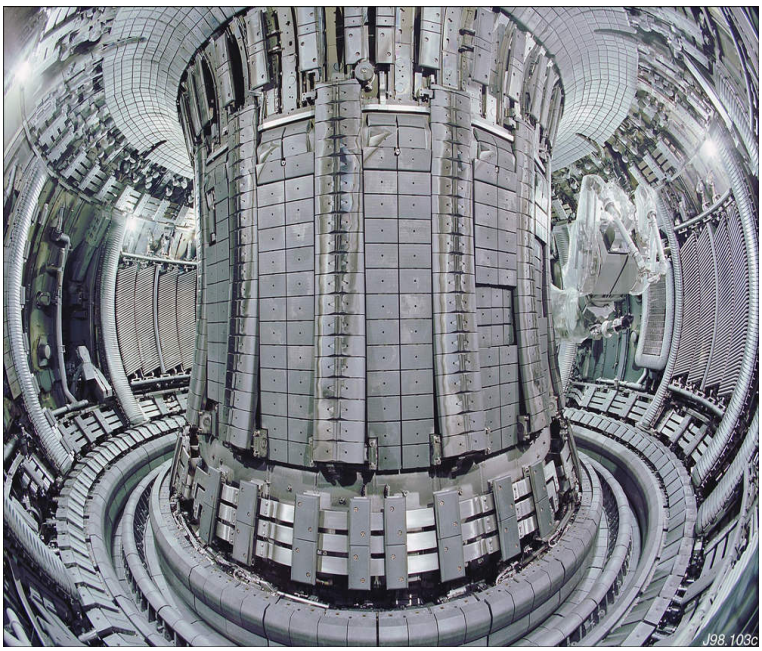


Figure 1.2: An image of the inside of the JET tokamak.

Spectroscopy can be divided into the broad categories of 'wavelength' and 'intensity' based spectroscopy. Wavelength spectroscopy takes wavelength information such as line centroids and line widths and returns information on the local plasma conditions such as flow velocities, ion temperatures and in certain circumstances ion and electron densities. It does this primarily via knowledge of the plasma distribution functions and relates the wavelength information to the appropriate plasma parameters, for example relating the shift in a line centroid to a doppler shift in the emitting atoms. In general it is not necessary to know detailed information on the atomic populations for such techniques. This is mostly, but not always, the case. For example, diagnosing plasma electron densities from observed collisionally broadened line widths requires information on the populations for the line broadening calculations. However, broadly speaking, these techniques are independent of the population distribution within the emitting atoms. The observations of such spectra developed alongside the models which use wavelength spectroscopy for their interpretation.

This thesis focuses largely on using intensity spectroscopy as a means of interpreting observational data. In intensity spectroscopy information such as line heights or line

ratios are used. The height of spectral lines is strongly dependent on the atomic population structure of the emitting atoms, thus models designed as tools for intensity spectroscopy are firmly grounded in atomic population modelling. Again the diagnostic models have tracked the development of observations and the increasing resolution to which spectra can be observed.

Initially it was mainly the strong resonance lines which could be resolved and intensity spectroscopy was used to relate the intensities of such lines to the population structure, which could then be related to the plasma emitter or electron densities and temperatures if information was available on all of the dominant atomic processes which determine the system's population distribution. The resonance lines of interest tended to come from plasmas of the coronal type, and as such could be modelled relatively simply. There were no optical thickness effects and the dominant atomic processes that had to be considered were largely the strong dipole-allowed collisional and spontaneous rates which determined the populations of the principal quantum shells. With the breadth in the wavelength range of spectrometers, observations could be made of most regions of interest and so most of the main resonance lines could be observed. Note that the general method in developing the diagnostic technique was to construct the atomic model, with all the appropriate transition rates, to then follow this through to a synthetic spectrum, or at least a theoretical intensity. A synthetic spectrum generated for intensity spectroscopy analysis is referred to as a 'spectral feature'. The optimisation of a fit of this feature to an observed spectrum returns a diagnostic of plasma parameters such as temperature, density, etc.

As plasmas of greater density (or sometimes of greater dimensions in the astrophysical case) were observed, optical thickness effects became significant. For example investigations into solar prominences led to the conclusion not only that they were extremely optical thick in the Lyman series (Hirayama, 1963), but that absorption of the Lyman continuum was one of the main sources for prominence energy gain (Poland and Anzer, 1971). The need to interpret optically thick spectra led to the development of various techniques to deal with opacity adjustments to populations, line shapes and emergent fluxes. These techniques can be broadly categorised into 'radiative transfer' and 'escape factor' methods and will be discussed later in this

chapter, and in chapter 2.

As spectroscopic techniques advanced it became possible to resolve finely split multiplets of known atomic systems. This allowed the redistributive rates between these finely split levels to be examined and atomic models were developed to account for such transition rates. The effects of re-distributive electron and ion collisions were included in the atomic modelling such that non-statistical, resolved populations could be evaluated. These models could then be employed to interpret the intensity of the observed spectral multiplet in terms of the dominant plasma parameters involved in the re-distributive transitions (such as the ion and electron densities). In this way more detailed plasma information than was possible using resonance lines alone could be diagnosed.

As more exotic plasmas were generated on earth and spectral observations of astrophysical objects improved, it became possible to observe the comparatively weak spectral lines originating from high quantum shells. These observed high series lines are often blended with neighbouring members and are typically observed from low temperature, high density plasmas. These spectra were first of all interpreted using wavelength spectroscopy (the wavelength of the last observable discrete line was used to determine the plasma electron density, see Inglis & Teller, 1939). Techniques were then developed such that intensity spectroscopy could be performed on series limit observations (Pigarov et al., 1998). Interpreting these spectra requires knowledge of the atomic processes to and from the high quantum shells, with a need to account properly for the transitions from high series blended lines and the smooth merging of such high n-shell bound populations through to free states. Account must also be taken of plasma microfield effects on the high lying populations and associated transitions consistently within the collisional-radiative framework. Such models can reap a further level of diagnostic information than was possible from resonance line or multiplet analysis alone. The work of this thesis is part of the development of this latest spectroscopic technique and seeks to match absolute intensities of high series observations with a fitted theoretical spectrum. Again the basic principle has been used where the construction of an atomic model leads to a predicted spectrum, allowing a fitting of this synthetic feature to the observations to be made and plasma

parameters diagnosed.

The next observational stage in fusion tokamaks is to look at the spectra produced by heavy species introduced to the plasma. This is as a result of the plans to layer heavy species into certain wall-tiles of the ITER reactor. There is a dual purpose in this, firstly these heavy species are more temperature resistant that the carbon based tiles that are used in existing reactors. Secondly these heavy species layers will provide a means of detecting how eroded the walls are at any point. The idea is that when the fusion plasma exposes the heavy species layers, they will be ejected into the reactor. These species will then emit characteristic spectra which will be used to alert the operators of the device to the progress of the wall erosion. Light species could not be used for this because they would be fully ionised in the core and would emit no spectral lines. In the build up to the ITER reactor there will be preparatory observations of heavy species high series limits as well as the extremely detailed grass-like spectra observed from the complex set of energy levels possible in such systems. For meaningful intensity spectroscopy to be performed on these new observations, it is necessary to develop a new atomic model. The later work presented in this thesis seeks to do this. The high series hydrogenic population work developed here can be used to account for the high lying populations in the heavy species and the basic plans are laid out which will allow the lower levels to be dealt with consistently. The basic methodology of intensity spectroscopy is adhered to, that is the atomic model developed will be carried through to a final spectrum which can be compared with observations to return diagnostic information on the heavy species emitters. Both the high series and heavy atom modelling introduce some difficulties which need to be dealt with. However, there is a corresponding return in the certainty and variety of diagnosed plasma parameters using these new models.

There were a variety of physical processes that required attention in this thesis. These included opacity, continuity of rates and populations from bound to free states, obtaining high quality line profiles for transitions near the series limit and dealing with the rate expressions for high quantum shell populations to greater resolution than has been done before. Before proceeding with a description of the basic theory used

throughout this thesis it is worthwhile stopping to overview each of these difficulties that must be overcome, describing in broad terms the physical nature of each problem.

Opacity refers to the process where photons travelling through a plasma do not escape, but are re-absorbed within the plasma volume. This has the dual effect of altering the emergent flux and adjusting the population distribution within the absorbing atoms. Although the emergent flux is usually reduced, it is possible for opacity to increase the flux in a given line if photo-absorptions in another line indirectly increase the population density of the upper level of the transition in question. If the photons escape without re-absorption occurring the plasma is said to be 'optically thin' in that transition. If such re-absorptions do occur it is referred to as being 'optically thick'. Opacity in principle couples every point in the plasma together and we have a non-linear and non-local problem to solve. The main approaches that have been developed to model opacity are 'radiative transfer' and 'escape factor' techniques. The technique of radiative transfer is a heavily computational approach to solving the coupled equations of radiative transfer and statistical balance. It has been used to deal with the effects of opacity on population structure, line profiles and emergent fluxes for various plasmas such as stellar atmospheres (Carlson, 1986) and solar prominences (Gouttebroze et al., 1993). The escape factor approach is a moderate optical depth method where it is appropriate to treat the equation of radiative transfer in a linear approximation. This approach has the advantage that it is easily integrated into other models, and has been used to diagnose optical depths in the solar atmosphere (Doyle & McWhirter, 1980, Brooks et al., 2000), to infer information on the structure of the solar atmosphere (Fischbacher, et al., 2000) and to diagnose plasma densities in fusion divertors (Behringer, 1998). See Irons (1979) for an overview of the basic escape factor expressions and derivations.

In this thesis opacity is accounted for using the escape factor approach. As will be seen, the approach is easily integrated into collisional-radiative models and emergent flux calculations. Escape factors are usually applied to discrete, low series member spectral lines (though not always, see Drawin (1970) for an example of escape factors used to account for continuum opacity). This thesis extends this low level approach

to model opacity through high series members into the continuum. We show that the effects of opacity continue smoothly from bound to free states in a similar manner to Gaunt factors and Saha-Boltzmann deviation factors (b-factors). This allows the usual low series member escape factor techniques to be extended to smoothly account for opacity in high series members through to the continuum.

In order to correctly predict the high series spectrum we also need to accurately model all the possible transition rates that can influence the high quantum shell populations. That is, one must account for all the possible transition rates (i.e. spontaneous, stimulated and collisional rates) that have an influence on the high lying atomic states. The modelling of atomic population distributions has a long history and is now at an advanced stage. The most successful technique in dealing with population distributions has been that of collisional-radiative theory (Bates et al., 1962) (see section 1.2.6 for a more complete description of the collisional-radiative approach). In this thesis the advancements to existing collisional-radiative models are performed within the framework of the Atomic Data and Analysis Structure (ADAS) suite of computer codes (Summers, 2001). ADAS consists of an interconnected set of computer codes and atomic data. The data represents the highest quality available, covering most types of data needed for existing astrophysical and fusion calculations. Standard ADAS data formats (referred to as 'adf' datafiles) are designed such that the codes are general purpose and applicable to a wide range of atomic and ionic systems. The codes are split into eight series with each series consisting of a set of codes. For example, series three contains the codes for charge exchange modelling. ADAS 311 then represents code eleven of series three. The codes are used to model the radiative properties for wide range of plasma conditions. The routines are designed such that they can solve for the populations in a number of 'pictures', whether in a b-factor, b-factor with exponential term included or c-factor form. This eliminates likely numerical inaccuracies and the computational techniques have been proven to be both stable and fast. The codes are also able to interpret spectral measurements and, within the series six set of codes, to generate synthetic spectra (referred to as 'special features'). We find it convenient to define a heirarchy of spectral features closely linked to population structure. If a set of lines in the special feature are

connected via pure branching line ratios they are referred to as 'feature primitives'; if the connection is via excited level population balance they are called 'features'; if the connection is via ionisation balance they are called 'superfeatures'. It is shown later how similar heirarchical ideas (section 4.1.1) in population structure lead to coherent organisation of complex atom modelling.

The ADAS codes are accessed through an IDL graphical user interface. This allows the user to specify which atomic system is to be investigated, what atomic data to use, what plasma parameters the code has to be run for and what format the output data and graphs are to be given in. This allows the user to immediately see the results of the calculation, making it possible to explore the parameter space for the given system. If there is no atomic data present for a given calculation it is possible to generate the necessary data (often to a lower quality) using various ADAS routines. For example ADAS 701 runs the autostructure code (Badnell, 1986), developed from the superstructure code (Eissner et al., 1974); ADAS 801 runs the Cowan structure code (Cowan, 1981) tailored to produce files of ADAS data format by O'Mullane; ADAS 211 generates radiative recombination data using the Gaunt factors developed in (Burgess & Summers, 1987). ADAS also contains a library of key subroutines that can be called from the user's own codes to assist in specific calculations.

This thesis contains a complete description of a model in progress that will form part of the ADAS suite of codes. This model will accurately predict the population structure of arbitrary heavy species and can be run in its present state to model high level hydrogenic populations. A module of this code is used to predict the high quantum shell populations needed for the spectral feature work of chapter 5.

The other main issue addressed in this thesis is the accurate modelling of high series line profiles. Historically, line profiles have been used to provide a wide range of plasma diagnostic information. Any broadened spectral line contains information on the physical process that contributed to the broadening. For example, doppler half-widths can be used to diagnose a plasma ion temperature and profile shapes can be used to infer the nature of the collisional broadening that produced the lineshape (i.e. whether electron or ion broadening dominates). The calculation of line profiles, in particular collisionally broadened line profiles, is a non-trivial problem with many

physical processes potentially contributing to the broadening of such lines. The situation is further complicated for high series lines due to the relatively small amount of high series observational data upon which to test the line profile calculations. Nevertheless, high quality line profile codes such as the PPP code (Talin et al., 1995), have been developed and have proven themselves to be reliable and valid for a wide range of plasma conditions.

Once all of these issues have been dealt with it is possible to combine the high series line profiles which continue smoothly through to continuum wavelengths with high level population results to generate a complete synthetic spectral feature at series limit wavelengths for a wide range of plasma conditions.

The rest of this chapter consists of a brief step back from this final picture and reviews the history of our approach to considering high series spectral prediction. It is hoped that this will provide a useful overview of all the physical effects and theoretical issues that have to be accounted for as well as showing the observations that led to the construction of the final model. Thus the next section provides some of the background theory that will be required, some of the theory is then developed in section 1.3 in the context of various spectral obsevations, from solar through to fusion plasmas.

Chapter 2 then goes into detail on the discrete low series spectral line opacity theory and the code known as ADAS 214 that is used to evaluate opacity modifications to both the emergent flux and atomic population structure of optically thick plasmas. Chapter 3 describes the extension of this theory to high series and continuum frequencies. Chapter 4 goes into the details of the high n-shell population model and our future plans for this collisional-radiative work. Chapter 5 then brings this all together and demonstrates the generation of an arbitrary high series spectral feature. Finally chapter 6 summarises our main conclusions and outlines the future direction of this work.

## 1.2 Background theory

### 1.2.1 Escape factor basic definitions

It is first useful to introduce some basic theory which can then be used as the building blocks for the developments presented in later chapters. The terminology of Fischbacher et al. (2000), and the notation of Irons (1979) are used throughout this thesis. Thus the following definitions hold:

- Transmission factor [T] - The average probability that a photon within the line profile will propagate from one given point to another.
- Escape Probability [$\Theta$] - Defined identically to the transmission factor except that the second point lies outside the plasma. That is, $\Theta$ is the average probability of a photon emitted within the line profile escaping from the plasma along a particular line of sight.
- Escape Factor - The mean probability that a line photon emitted somewhere in the plasma will escape from the plasma along any line of sight. The phrase 'escape factor technique' is also used in this thesis to describe the general technique of linearising the equation of radiative transfer for the evaluation of the expressions defined here.
- Absorption factor [$\Lambda$] - one minus the probability that a net absorption of a photon will occur at a particular point in a plasma. This is sometimes referred to as the 'Biberman-Holstein coefficient' or 'net radiative bracket'.

Note that the only difference between these definitions and those of Irons is that he defines the escape probability to be the mean probability of a photon emitted at a point in a plasma escaping along any line of sight. This is the same as the escape probability defined as above averaged over solid angle. It is felt that defining the escape probability along one given line of sight is an expression more directly applicable to actual observations.

### 1.2.2 Escape probability and emergent flux

Considering the observed flux escaping from a plasma then the equation of radiative transfer is used to model the variation of the radiation intensity ($I$) along a given line of sight, denoted by the points along $l$.

$$\frac{dI(\nu,l)}{dl} = \varepsilon(\nu,l) - \alpha(\nu,l)I(\nu,l) \tag{1.1}$$

where

- $\varepsilon(\nu,l)$ is the emission coefficient defined as the number of photons emitted at frequency $\nu$ per unit time, per unit volume, per unit solid angle at position $l$.
- $\alpha(\nu,l)$ is the absorption coefficient, defined such that $\alpha(\nu,l)I(\nu,l)$ is the number of photons absorbed at frequency $\nu$ per unit time, per unit volume, per unit solid angle at position $l$.
- $I(\nu,l)$ is the intensity of the radiation field at the point of interest ($l$), defined as the number of photons crossing a unit area, per unit time, per unit solid angle, per unit frequency.

Also define the optical depth ($\tau$) of the plasma to be the absorption coefficient integrated along the line of sight. Thus the optical depth is given by the following expression, with the simplified result for a constant absorption coefficient also shown.

$$\begin{aligned} \tau(\nu) &= \int_0^b \alpha(\nu,l)dl \\ &= \alpha(\nu)b \end{aligned} \tag{1.2}$$

This gives an indication of how far one can 'see' into the plasma. It should be noted that equation (1.1) is non-linear because the emission coefficient ($\varepsilon$) at point $l$ depends upon the upper level population density of the transition in question. This in turn depends upon the number of photo-absorptions that can excite an electron into this level, which depends upon the radiation field $I$ at point $l$, thus making $\varepsilon$ in principle a function of $I$ and thus equation (1.1) non-linear. Note that the emission coefficient

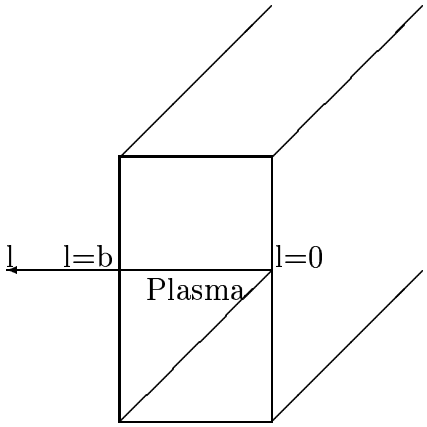


Figure 1.3: Diagram of the line of sight used in the escape probability formalism.

at $l$ in principle depends upon $\varepsilon$ at all the other points in the plasma (due to the dependence of the populations at $l$ upon the local radiation field and hence upon the emission from elsewhere in the plasma) making the equation non-local as well. The method employed throughout this thesis is to solve the equation of radiative transfer by assuming that the emission coefficient is independent of the intensity term, thus making equation (1.1) linear and allowing it to be solved using an integrating factor approach. This assumption of linearity will be reasonable for plasmas which are not significantly optically thick and thus do not have a large degree of spatial coupling. Consider a line of sight through a plasma with the origin at the back face as in figure 1.3. Consider first of all a purely absorbing plasma with a constant absorption coefficient and with incident intensity $I(\nu, 0)$, the intensity observed at $b$ will be given by

$$I(\nu, b) = I(\nu, 0)e^{-\int_0^b \alpha(\nu) dl} \tag{1.3}$$

If $\alpha$ is allowed to vary with respect to $l$ and the plasma can also emit along the line of sight the emergent intensity will be

$$I(\nu, b) = \int_0^b \varepsilon(\nu, l) e^{-\int_l^b \alpha(\nu, l') l' dl'} dl + I(\nu, 0) e^{-\int_0^b \alpha(\nu, l) dl} \tag{1.4}$$

The emission and absorption coefficients are given by

$$\varepsilon(\nu, l) = \frac{1}{4\pi} A_{n' \to n} N_{n'}(l) \theta(\nu, l) \tag{1.5}$$

and

$$\begin{aligned} \alpha(\nu, l) &= B_{n \to n'} N_n(l) \theta(\nu, l) \\ &= N_n(l) \frac{c^2}{8\pi} \left( \frac{n'}{n} \right)^2 \frac{1}{\nu^2_{n' \to n}} A_{n' \to n} \theta(\nu, l) \end{aligned} \tag{1.6}$$

with

- $A_{n' \to n}$ = the Einstein-A value for the spontaneous emission $n' \to n$ $[s^{-1}]$
- $N_{n'}$ = Atomic population of level $n'$ $[cm^{-3}]$
- $N_n$ = Atomic population of level $n$ $[cm^{-3}]$
- $\theta(\nu)$ = emission profile which is assumed equal to the absorption profile [s]
- $B_{n \to n'}$ = Einstein-B value for photo-absorption $n \to n'$ $[cm^2 s^{-1} sr^{-1}]$

To see the definition of the escape probability the line integrated emergent flux at b is written as follows:

$$\begin{aligned} I(b) &= \int_{line} \left[ \int_0^b \varepsilon(\nu, l) e^{-\int_l^b \alpha(\nu, l') dl'} dl + I(\nu, 0) e^{-\int_0^b \alpha(\nu, l) dl} \right] d\nu \\ &= \frac{\int_{line} \int_0^b \varepsilon(\nu, l) e^{-\int_l^b \alpha(\nu, l') dl'} dl d\nu + \int_{line} I(\nu, 0) e^{-\int_0^b \alpha(\nu, l) dl} d\nu}{\int_{line} \int_0^b \varepsilon(\nu) dl + I(\nu, 0) d\nu} \\ &\quad \times \int_{line} \int_0^b \varepsilon(\nu) dl + I(\nu, 0) d\nu \\ &= \Theta_{n \to n'} \int_{line} \left[ \int_0^b \varepsilon(\nu) dl + I(\nu, 0) \right] d\nu \\ &= \Theta_{n \to n'} \left[ \frac{1}{4\pi} A_{n' \to n} \int_0^b N_{n'}(l) dl + \int_{line} I(\nu, 0) d\nu \right] \end{aligned} \tag{1.7}$$

Thus the escape probability, $\Theta$, is defined as the ratio of the opacity modified escaping flux to the optically thin escaping flux, with both fluxes evaluated as line integrated values. That is,

$$\Theta_{n\to n'} = \frac{\int_{line}\int_0^b \varepsilon(\nu,l)e^{-\int_l^b \alpha(\nu,l')dl'}dld\nu + \int_{line} I(\nu,0)e^{-\int_0^b \alpha(\nu,l)dl}d\nu}{\int_{line}\int_0^b \varepsilon(\nu)dl + I(\nu,0)d\nu} \tag{1.8}$$

This is our general escape probability expression from which we derive all further results. In chapter 2 this expression is developed and evaluated for various plasma geometries and line profiles and in chapter 3 it is extended to include continuum frequencies.

The escape probability can be used as a parametric adjustment on the spontaneous emission coefficient allowing the line integrated emergent flux of a discrete spectral line transition, $n \to n'$, to be written as

$$I = \frac{1}{4\pi}\Theta_{n\to n'}\left[A_{n'\to n}\int_0^b N_{n'}(l)dl + \int_{line} I(\nu,0)d\nu\right] \tag{1.9}$$

### 1.2.3 Absorption factor and populations

Consider now the opacity effects from the perspective of atomic population modification. Writing out the spontaneous emission rate from level $n'$ to $n$, and photo-absorptions to $n'$ from $n$ we get the following expression for the net photo-emission rate contribution to the statistical balance equations

$$\int_\Omega\int_{line}\varepsilon_{n'\to n}(\nu,l)d\nu d\Omega - \int_\Omega\int_{line}\alpha_{n\to n'}(\nu,l)u(\nu,l)d\nu d\Omega \tag{1.10}$$

where one considers emission from a volume element and photo-absorption to this element, neglecting stimulated emission, and $u(\nu,l)$ is the radiation density at $l$. Assuming that the emission from the volume element is uniform in all directions and integrating over the normalised emission profile, the net spontaneous emission rate is

$$\int_\Omega\int_{line}\varepsilon_{n'\to n}(\nu,l)d\nu d\Omega - \int_\Omega\int_{line}\alpha_{n\to n'}(\nu,l)u(\nu,l)d\nu d\Omega \tag{1.11}$$

$$= \int_\Omega \int_{line} \varepsilon_{n'\to n}(\nu,l)d\nu d\Omega \left[1 - \frac{\int_\Omega \int_{line} \alpha_{n\to n'}(\nu,l)u(\nu,l)d\nu d\Omega}{\int_\Omega \int_{line} \varepsilon_{n'\to n}(\nu,l)d\nu d\Omega}\right] \quad (1.12)$$

$$= \Lambda_{n\to n'}(l) \int_\Omega \int_{line} \varepsilon_{n'\to n}(\nu,l)d\nu d\Omega \quad (1.13)$$

That is

$$\Lambda_{n\to n'}(l) = 1 - \frac{\int_\Omega \int_{line} \alpha_{n\to n'}(\nu,l)u(\nu,l)d\nu d\Omega}{\int_\Omega \int_{line} \varepsilon_{n'\to n}(\nu,l)d\nu d\Omega} \quad (1.14)$$

$\Lambda_{n\to n'}$ is referred to as the absorption factor, following the terminology of Fischbacher et al. (2000). It can be seen that $\Lambda_{n\to n'}$ is one minus the total number of photo-absorptions at $\underline{r}$ divided by the total number of spontaneous emissions at $\underline{r}$. That is $\Lambda_{n\to n'}(l)$ represents the probability of a photon not being absorbed at position $l$ in the plasma.

It is interesting to consider the limiting case of a black body. In this case the radiation density $u(\nu)$ is given by the source function equivalent to $\varepsilon(\nu,l)/\alpha(\nu,l)$. Also, if the plasma is a black body throughout its volume then $\alpha(\nu,l)$ and $\varepsilon(\nu,l)$ are independent of position. That is

$$\begin{aligned} \Lambda_{n\to n'}(l) &= 1 - \frac{\int_\Omega \int_{line} \alpha_{n\to n'}(\nu)\frac{\varepsilon(\nu)}{\alpha(\nu)}d\nu d\Omega}{\int_\Omega \int_{line} \varepsilon_{n'\to n}(\nu)d\nu d\Omega} \\ &= 0 \end{aligned} \quad (1.15)$$

Thus we have complete re-absorption of all emitted photons at any point $l$ as expected from detailed balance under thermodynamic equilibrium conditions.

Note that for the absorption factor argument here we are considering absorption and emission at a point in the plasma. It is no longer the escaping flux that is of interest but the population modification at the point $l$. The photo-absorption transition rate can be absorbed into the spontaneous emission rate by including the absorption factor as a parametric adjustment. That is, photo-absorptions are included as negative spontaneous emissions. In our collisional-radiative calculations this is evaluated by multiplying the Einstein A-value for each transition by its corresponding absorption factor. Hence when one solves the statistical balance equations including these absorption factors the opacity modified population structure is produced.

The absorption factor expression of (1.14) is our starting expression for the opacity modifications to population structure. It is developed in chapter 2 for various geometries and line profiles. Chapter 3 then provides the extension of this expression to continuum frequencies.

Thus we have two basic expressions, (1.8) and (1.14), which can be used to account for the effects of opacity in an optically thick plasma.

### 1.2.4 Continuum opacity

There is of course a continuum equivalent to the discrete line opacity that we have looked at. Here we consider photo-ionisations and recombinations rather than photo-absorptions and spontaneous emissions. See Drawin (1970) for an example of continuum absorption factors derived and used in practice (in his case to evaluate plasma relaxation timescales). The continuum escape probability, which will also be referred to as the bound-free escape probability, is derived below. Note the similarities with the bound-bound expression.

The continuum integrated flux at b is written as

$$\begin{aligned} I(b) &= \int_{contm} \left[ \int_0^b \varepsilon_{bf}(\nu,l) e^{-\int_l^b \alpha_{bf}(\nu,l')dl'} dl + I(\nu,0) e^{-\int_0^b \alpha_{bf}(\nu,l)ldl} \right] d\nu \\ &= \frac{\int_{contm} \int_0^b \varepsilon_{bf}(\nu,l) e^{-\int_l^b \alpha_{bf}(\nu,l')dl'} dl d\nu + \int_{contm} I(\nu,0) e^{-\int_0^b \alpha_{bf}(\nu,l)ldl} d\nu}{\int_{contm} \int_0^b \varepsilon_{bf}(\nu) dl + I(\nu,0) d\nu} \\ &\quad \times \int_{contm} \int_0^b \varepsilon_{bf}(\nu) dl + I(\nu,0) d\nu \\ &= \Theta_n \int_{contm} \int_0^b \varepsilon_{bf}(\nu) dl + I(\nu,0) d\nu \\ &= \Theta_n \left[ \frac{1}{4\pi} A_{\kappa \to n} \int_0^b N_\kappa(l) dl + \int_{contm} I(\nu,0) d\nu \right] \end{aligned} \tag{1.16}$$

Note that $\kappa$ represents the extension of bound states, $n'$, into the continuum via the transformation $n' \to i\kappa$. The bound-free emission and absorption coefficients are taken from Menzel & Pekeris (1935). That is

$$\begin{aligned} \varepsilon_{bf}(\nu)d\nu &= \frac{1}{4\pi}\left[N_i f(v) b_\kappa dv\right]\left[N_e v \sigma_{\kappa n}\right] \\ \Rightarrow \varepsilon_{bf}(\nu) &= \frac{1}{4\pi}\left[N_i f(v) b_\kappa dv\right]\left[N_e v \sigma_{\kappa n}\frac{1}{d\kappa}\right]\frac{d\kappa}{d\nu} \end{aligned} \tag{1.17}$$

and

$$\alpha_{bf}(\nu) = N_n \frac{\pi e^2}{mc} f'_{n\kappa}\frac{d\kappa}{d\nu} g^{II}_{n\kappa} \tag{1.18}$$

where $f(v)$ is the Maxwellian velocity distribution for free electrons, $\sigma_{\kappa n}$ is the target area for free electron capture given by

$$\sigma_{\kappa n} = \frac{2^4}{3\sqrt{3}}\frac{e^2 h}{m^2 c^3}\frac{1}{\left[\frac{1}{n^2}+\frac{1}{\kappa^2}\right]}\frac{\kappa^2}{n^3} g^{II}_{\kappa n} \tag{1.19}$$

$f'_{n\kappa}$ is the bound-free oscillator strength and $g^{II}_{n\kappa}$ is the bound-free Gaunt factor.
Thus the escape probability $\Theta_n$ is defined as the ratio of the opacity modified escaping flux to the optically thin escaping flux, with both fluxes evaluated as continuum integrated fluxes. It follows that

$$\Theta_n = \frac{\int_{contm}\int_0^b \varepsilon_{bf}(\nu,l) e^{-\int_l^b \alpha_{bf}(\nu,l')dl'} dl d\nu + \int_{contm} I(\nu,0) e^{-\int_0^b \alpha_{bf}(\nu,l)dl} d\nu}{\int_0^b \int_{contm} \varepsilon_{bf}(\nu)d\nu + I(\nu,0)dl} \tag{1.20}$$

Note that there is no subscript $\kappa$ on $\Theta_n$ in the definition shown here. This is because the escape probability is integrated over the whole set of continuum states $\kappa$, thus $\Theta_n$ represents the probability of a recombination photon, produced from an electron anywhere in the continuum recombining to the state $n$, escaping along the chosen line of sight. A more general expression that is not integrated over the whole continuum is presented in chapter 3.
In a similar manner the absorption factor for bound-free transitions may be written in its general form. The net ionisation rate is given by

$$\int_\Omega \int_{contm} \varepsilon_{\kappa\to n}(\nu,l) d\nu d\Omega - \int_\Omega \int_{contm} \alpha_{n\to\kappa}(\nu,l) u(\nu,l) d\nu d\Omega \tag{1.21}$$

$$= \int_{\Omega}\int_{contm} \varepsilon_{\kappa\to n}(\nu,l)d\nu d\Omega \left[1 - \frac{\int_{\Omega}\int_{contm} \alpha_{n\to\kappa}(\nu,l)u(\nu,l)d\nu d\Omega}{\int_{\Omega}\int_{contm} \varepsilon_{\kappa\to n}(\nu,l)d\nu d\Omega}\right] \quad (1.22)$$

$$= \Lambda_{n\to\kappa}(l)\int_{\Omega}\int_{contm} \varepsilon_{\kappa\to n}(\nu,l)d\nu d\Omega \quad (1.23)$$

where the absorption and emission coefficients have the same definitions as in the bound-free escape factor case. That is, the absorption factor for bound-free photo-absorption is given by

$$\Lambda_{n\to\kappa}(l) = 1 - \frac{\int_{\Omega}\int_{contm} \alpha_{n\to\kappa}(\nu,l)u(\nu,l)d\nu d\Omega}{\int_{\Omega}\int_{contm} \varepsilon_{\kappa\to n}(\nu,l)d\nu d\Omega} \quad (1.24)$$

The similarity between equations (1.20), (1.24) and the bound-bound counterparts (1.8), (1.14) is clear. This similarity is shown formally in chapter 3 where the bound-bound expressions are shown to analytically continue into the bound-free ones upon application of the transformation $n' \to i\kappa$.

### 1.2.5 Line broadening

In practice it is found that the escape probability and absorption factor expressions can be highly sensitive to the emitting and absorbing line profiles, see for example the illustrations in Behringer (1998). For this reason, and in order to accurately compare any theoretical spectrum (whether optically thin or thick) with that observed it is necessary to model emission and absorption line profiles with a high degree of precision. This is especially true for the high series work presented in chapter 5 where the theoretical electron broadened line widths are used as a density diagnostic. There are many standard textbooks which give an overview of the basic theory behind line broadening (see Griem, 1974, Griem, 1997, Sobelman et al., 1981 and chapter 13 of Bates, 1964). Most work in this area concentrates on the evaluation of pressure broadening as it is the most complex and often the most important line broadening mechanism. The next few sections will give a brief overview of the main broadening expressions, concentrating on a description of the physical processes behind each mechanism. The following sections will lay out the background theory necessary to put the line profile calculations of chapters 2, 3, 4 and 5 into context. There exists a

wide range of broadening mechanisms including Doppler broadening, natural broadening, pressure broadening as well as instrumental effects which alter the observed profile. The basic line profile expressions for each of these mechanisms are presented along with any approximate expressions that are used in the later chapters.
In practice one usually assumes that the emission and absorption profiles are identical. That is, in the time from photo-absorption to subsequent re-emission, there have been sufficient collisions such that the direction of the emitted photon is not related to that from which it was absorbed. Thus the emitted photon has been thermalised and the resultant emission profile is governed by the same plasma properties that lead to the absorption profile. This assumption is often referred to as complete frequency redistribution (CRD) and is made throughout the rest of the thesis with the possibility of different emission and absorption profiles being included at a future date if necessary.

### Temperature effects

The broadening due to the inherent thermal motion of the emitting or absorbing atoms, provided their velocity distribution is Maxwellian with characteristic temperature T, results in a line profile given by the normalised Doppler expression

$$\theta(\nu) = \frac{1}{\sqrt{\pi}\Delta\nu_D} e^{-\left(\frac{\nu-\nu_0}{\Delta\nu_D}\right)^2} \tag{1.25}$$

where

$$\Delta\nu_D = \frac{1}{\nu_0}\sqrt{\frac{2kT}{m}} \tag{1.26}$$

is the Doppler half width of the gaussian line profile.

### Natural broadening

There exists a mechanism usually referred to as natural broadening, resulting from the finite lifetime of the emitting atom in its excited state (as predicted by the Heisenberg uncertainty principle, $\Delta E \Delta t \approx h/2\pi$).

Natural broadening exists independently of any external influences on the emitting atom. It results in a profile known as Lorentzian with a width characterised by $\Delta\nu_L = A_{n'\to n}/2\pi$.
The profile expression is of the form

$$\theta(\nu) = \frac{(\Delta\nu_L)^2}{(\nu - \nu_0)^2 + 4(\Delta\nu_L)^2} \tag{1.27}$$

This broadening mechanism is negligible when compared to pressure and doppler broadening for the cases that are usually encountered in fusion and astrophysical plasmas.

**Density effects**

For dense plasma conditions it is likely that both natural broadening and doppler broadening will be negligible compared with the collisional broadening induced by the charged particles of the plasma, interacting through the Stark effect. Neutral broadening and the long range Van der Waals broadening will be neglected with only broadening due to electrons and ions being considered in this work. The most general expression for a Stark broadened line profile is

$$\theta(\omega) = \frac{1}{\pi} Re\left\{\int_0^\infty exp(i\omega s) C(s) ds\right\} \tag{1.28}$$

where $C(s)$ is referred to as the autocorrelation function of the light amplitude and is evaluated from quantum mechanical knowledge of the perturber and emitter. The complete treatment of such broadening is complicated by the fact that slow moving perturbers interact with the emitter in a different way to the faster perturbers. Usually one of two limiting approximations is used to account for the broadening effects of the charged perturbers. If the perturber is fast all the broadening collisions will be statistically independent from each other and can be individually accounted for. This is known as the 'impact approximation' (Lorentz, 1906) and leads to a Lorentzian profile. If the perturber is very slow then it can be considered to be stationary from the emitter's point of view and the broadening effects of the resultant field due to all

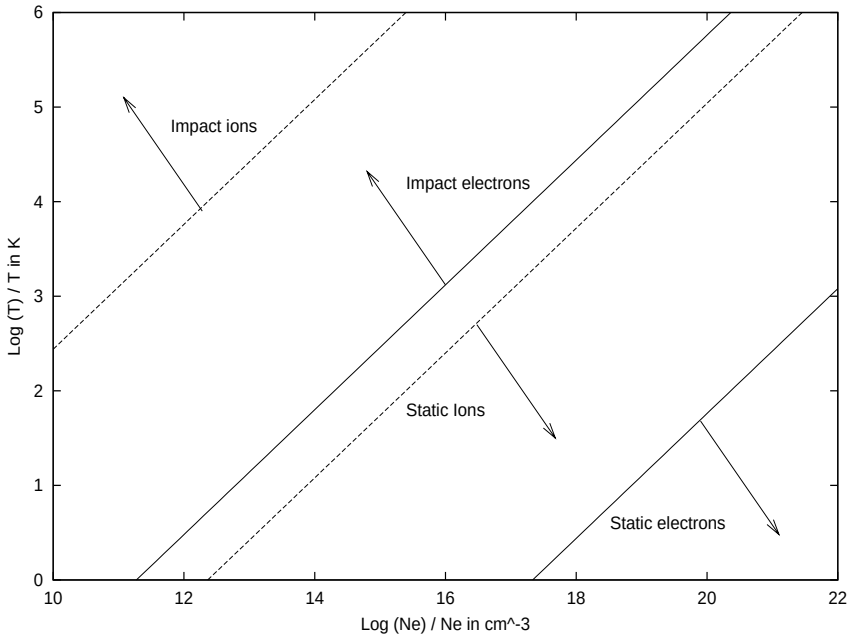


Figure 1.4: Range of validity of broadening approximations for $H\alpha$, taken from Stamm et al. (1998).

the 'stationary' perturbers estimated; this is referred to as the 'quasi-static approximation' (Holtsmark, 1919).

Both ions and electrons broaden the lines through the Coulomb interaction between themselves and the electrons in the emitting atom. Thus the only difference between the broadening effects of the ions and electrons comes from their differing speed, with the electrons typically having a much higher average thermal velocity than the ions. Thus typically the electrons are treated in the impact and the ions in the quasi-static approximation. It should be noted that reality does not always fall into either of these two limiting approximations, but in the intermediate regime between the two. In figure 1.4 an illustration of the boundaries of these two approximations for ions and electrons is shown for some plasma conditions likely to occur in practice. The arrows indicate the regimes for which the impact and quasi-static approximations are valid. Note that the graph is only valid for $H\alpha$, but could in principle be evaluated for any line.

### The impact approximation

As stated previously, the impact approximation assumes that collisions are statistically independent and thus the total broadening effect of the collisions can be evaluated from the sum of each broadening collision.

In practice the impact approximation is usually valid for the treatment of electron collisional broadening due to their fast thermal motion and thus the short timescale of their collisions with the emitting atom. This broadening in isolation produces a Lorentzian profile with characteristic half widths which are primarily functions of the perturber density. Griem (1960) derives a simplified expression for a transition from $n' \rightarrow n$ with an electron broadened half width given by

$$\gamma = 5.6 \times 10^{-6} N^{1/3} Z^{-1} T^{-1/2} \left[ log_{10} \left( \frac{4 \times 10^6 TZ}{n' N^{1/2}} \right) - 0.125 \right] \frac{n'^5 + n^5}{n'^2 - n^2} \qquad (1.29)$$

Note that if Doppler broadening is also significant then the resultant profile would be a convolution of a Lorentzian and Gaussian profile which is referred to as a Voigt profile. Such profiles are often available as tables, e.g. Allen (1991).

### The Quasi-static approximation

At the other extreme, it may be the case that the charged perturbers have negligible motion during the lifetime of the emitting upper level. Under these circumstances the effects of the perturbers can be best modelled as a field broadening the line. The quasi-static approximation is usually applied as follows. The perturbers are assumed to be stationary and one calculates the effect of the consequent static electric field on the lines via the Stark effect. One then accounts for the statistical distribution of the field by evaluating the probability distribution of the electric field. The Stark profiles are then averaged over this distribution.

The probability distribution of the ion electric field is usually denoted by $W(F)$ with $F = E/E_0$ and $E_0 = e/r_0^2$, where $r_0$ is the mean distance between particles in the plasma. This represents the probability that a certain electric field ($E$), due to the presence of surrounding ions, will be experienced by the emitting atom and is usually referred to as the 'statistical microfield distribution function'. These have

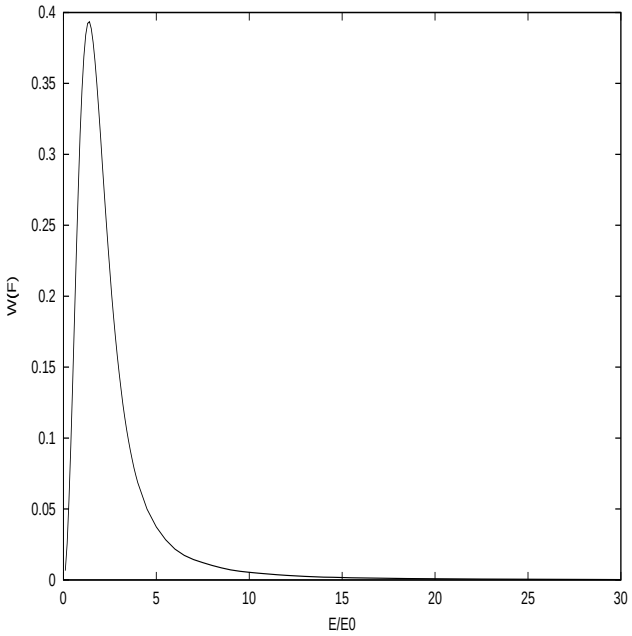


Figure 1.5: Ion-microfield plotted for plasma parameters as described in the text.

been widely evaluated in work such as that of Hooper (1966) and Hooper (1968). In the ideal gas limit they reduce to the Holtsmark field (Holtsmark, 1919). Figure 1.5 shows a microfield distribution function for a plasma consisting of 99% $D^+$ and 1% $D^0$ at an electron temperature of $1eV$ and an electron density of $1 \times 10^{14} cm^{-3}$. The APEX code (Iglesias, Lebowitz & McGowan, 1983) is used throughout this thesis in any microfield calculations. This routine is regarded as being highly accurate and is widely used; see chapter 3 of Griem (1997) for more details on the use of this code.
It is not normally appropriate to model the effects of the electrons using this technique. The ion collisions on the other hand are often modelled in this approximation. Their slower velocities means that they often fall into the regime where their interactions with the emitting atom are over long periods of time. In general a reasonable guide in determining the balance between the two approaches is that that the quasi-static approximation is valid if the linewidth is large compared with the inverse of a typical collision time, and the impact approximation is valid if this value is small when compared to the inverse of a typical collision time.
Note that in practice, one does not have only one broadening mechanism influencing

the line profile. In dense plasmas one is likely to get influences from both the electrons and the ions which must be simultaneously accounted for.

### Accounting for both ion and electron collisional broadening

In practice it is common to take the following approach. The emitting atom is assumed to lie in a constant electric field produced by the 'stationary' ions which produces a Stark broadened set of lines. These lines are then further broadened by electron collisions within the impact approximation. Finally the statistical distribution of the ionic field is accounted for by averaging the broadened set of lines with the probability distribution function of the ion field. Thus the electrons are accounted for using the impact approximation and the ions via the quasi-static approximation. The quantum mechanical form of this is shown below. One would then convolve the resulting profile with the Doppler profile and instrumental function if appropriate.

This process is evaluated numerically in the Pim Pam Poum (PPP) code (Talin et al., 1995, Talin et al., 1997). This code is well tested and provides an accurate evaluation of Stark broadened profiles due to ion and electron perturbers. The code takes in atomic data containing energy level information and spontaneous emission values as well as the set of plasma parameters for which the profile is to be evaluated and returns the emission coefficient for the transition of interest (i.e. $\frac{1}{4\pi}A_{n'\rightarrow n}N_{n'}\theta(\nu)$). The profile can be either normalised or not and the population density can be set to the Saha-Boltzmann values or a pre-calculated population density distribution used. Thus the PPP code, coupled with the ADAS collisional-radiative codes can provide accurate line profiles with absolute intensities for a wide range of plasma conditions. An example of a profile evaluated using the PPP code is shown in figure 1.6. The $9-2$ Balmer series line is shown for the case where only the electron broadening and then the ion plus electron broadening is considered. It can be seen that for these plasma conditions, the electron broadening dominates the line shape, although the ion broadening is still significant.

In the thesis work presented here a more approximate method which captures the main behaviour of all the broadening mechanisms is also used. This fast, approximate method is of use particularly in chapter 5 where a large number of hydrogen series

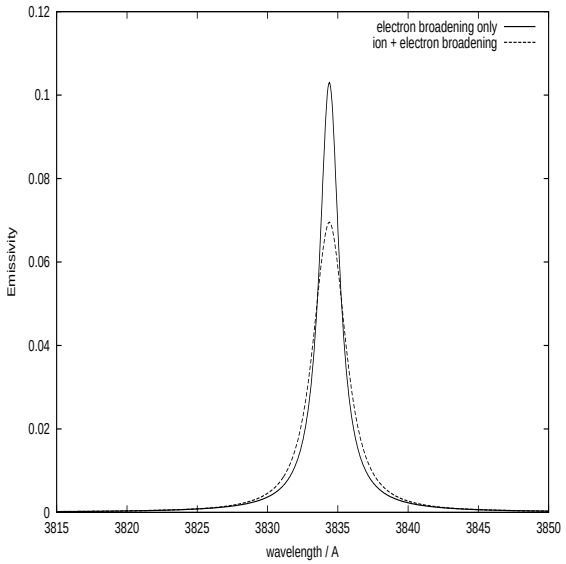


Figure 1.6: Example of the hydrogen 9-2 Balmer series spectral line profile as evaluated by the PPP code for an electron density of $1 \times 10^{14} cm^{-3}$ and an electron temperature of $1 \times 10^4 K$.

profiles need to be evaluated and the accuracy of the very high series member is not of primary importance. Griem (1960) derives a simplified algebraic expression for evaluating ion and electron broadened profiles for hydrogen, with the ions treated in the quasi-static and the electrons in the impact approximation. The same basic expression is also given in Sobelman et al. (1981). The expressions are designed to be quick to apply, using look-up tables which cover a reasonable range of electron and ion broadening half widths. The basic expression used is

$$I = \frac{1}{F_0} \frac{1}{K_{nn'}} T(\beta, \gamma) \tag{1.30}$$

$T(\beta, \gamma)$ is found from the look-up tables, $\gamma$ (the half width due to electron broadening) is evaluated from equation (1.29), $F_0 = 2.61 e N^{\frac{2}{3}}$ is the Holtsmark normal field strength, $K_{nn'} = 5.5 \times 10^{-5} Z^{-5} \frac{(nn')^4}{n'^2 - n^2}$ , $\beta = a / K_{nn'}$ with $a = \Delta\lambda / F_0$.
In evaluating this approximate expression an extension was made to make it more robust. As one progresses up a given series, electron broadening dominates, and the profiles tend towards Lorentzian profiles with their half-widths determined purely

by the electron broadening expression. Thus for values of $\beta$ that fall outside Griem's table, it was assumed that electron broadening dominated and a Lorentzian expression was used with a half-width given by $\gamma$. This is not always a valid approximation. For example if the ion broadening is still significant then the calculated line will not be as broad as it would in reality. As is shown in chapter 5, Griem's expression prove to be valid for many of the plasma conditions that are investigated in this thesis; see section 5.2.3 for more details.

Thus the preferred method for profile calculation in this thesis has been as follows. For simplified conditions, where Doppler or simple Lorentzian profiles are valid, no complex profile calculations are done. For conditions where significant Stark broadening occurs in both the ions and electrons, the PPP code is used, especially for lines that are to be used for diagnostic purposes. In chapter 5 very high hydrogen series member profiles must be evaluated. The approximate expression is used under such circumstances to supplement the PPP results for the low series member lines.

#### Optical thickness effects

It is also possible for opacity to modify a given observed line profile. On travelling through a plasma it is more likely that line centre photons will be absorbed as compared to those in the line wings. This can be seen from equation (1.8) for the absorption factor, where $\alpha$ is significantly higher at line centre as compared with the line wings. Thus the profile that finally emerges from the body of the plasma could have reduced intensity at the line centre, leading either to a line flattening or even a line inversion. See figure 1.7 for examples of this evaluated using ADAS 214 for the case of a parabolic density distribution within a cylindrical plasma.

### 1.2.6 Population modelling

The simplifying assumptions commonly made when modelling plasma atomic populations can best be understood upon consideration of the various atomic and plasma lifetimes. These lifetimes allow one to calculate an 'equilibrium time constant' describing the time taken for each plasma constituent to relax to its equilibrium state.

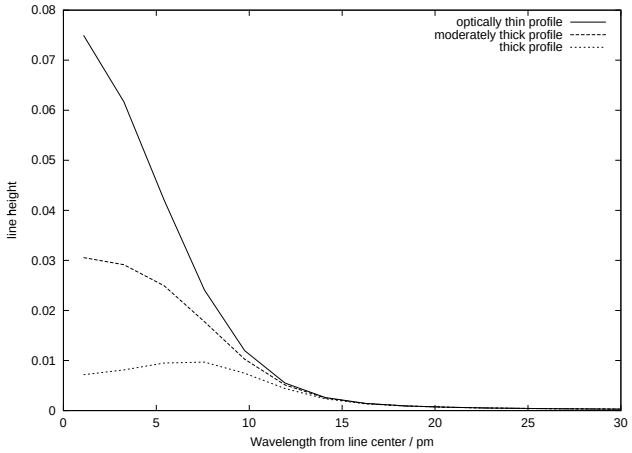


Figure 1.7: Examples of opacity modified line profiles evaluated using ADAS 214. The top profile is the optically thin one. The next lower one is the moderately thick case, note that its top is flattened. The lowest case is the optically thick case, note that its centre is inverted.

The relative values of these time constants determines the optimal atomic modelling approach. Define $\tau_{plasma}$ such that it describes the dynamical timescale of the plasma, that is the timescale upon which the typical plasma parameters vary (or often in the case of laboratory plasmas, the timescales for which the plasma exists). $\tau_{plasma}$ also describes the typical timescale for plasma particles to cross temperature and density scale lengths. Comparing the time constant for each plasma process with $\tau_{plasma}$ gives an indication of whether that process has time to equilibriate before the plasma conditions vary. Due to typical plasma confinement times $\tau_{plasma}$ is of the order of one second for the core plasma of a fusion tokamak and as low as $10\,ms$ for the divertor plasma. One can also define certain 'extrinsic' time constants, such as $\tau_{e-e}$, giving the time for electron-electron collisions to thermalise the free electrons, $\tau_{i-i}$ describing the equivalent ion-ion equipartition and $\tau_{i-e}$ for ion-electron equilibration (i.e. the time for the electron and ion distributions to reach the same characteristic temperature). Define $\tau_{ion}$ such that it describes the ionisation relaxation timescale for the plasma. There also exist certain 'intrinsic' time constants describing states within the atomic system under consideration. $\tau_m$ gives the relaxation time for the metastable states, $\tau_o$ for the ordinary excited states and $\tau_a$ for the auto-ionising states.

Before looking at typical values for each of these time constants, consider the case

where all of the intrinsic and extrinsic time constants are much less that $\tau_{plasma}$, the plasma is in isolation and there is no escaping radiation field. In this case the plasma is said to be in 'thermodynamic equilibrium' (TE) and each process is balanced by its inverse (referred to as the 'principle of detailed balance'). Under such conditions, the free plasma particles (electrons, ions etc) have Maxwellian velocity distributions characterised by the same temperature, described by

$$f(\mathbf{v}) = 4\pi \left(\frac{m}{2\pi kT}\right)^{\frac{3}{2}} e^{-(m\mathbf{v}^2)/(2kT)}\mathbf{v}^2 \tag{1.31}$$

The plasma internal radiation field is that of a black body and given by the Planck function:

$$u(\nu) = \frac{8\pi h\nu}{c^3}\left(e^{h\nu/kT} - 1\right) \tag{1.32}$$

and the bound states of the atoms and ions have Boltzmann distributions, such that the ratio of population densities of bound states $i$ and $j$ is given by

$$\frac{N_i}{N_j} = \frac{\omega_i}{\omega_j} e^{(I_i - I_j)/(kT)} \tag{1.33}$$

where $\omega_i$ and $\omega_j$ are the statistical weight of levels $i$ and $j$. The absolute populations of level $i$ are given by the Saha-Boltzmann equation

$$N_i = N_+ N_e \left(\frac{h^2}{2\pi mkT}\right)^{\frac{3}{2}} \frac{\omega_i}{2\omega_+} e^{(I_i)/(kT)} \tag{1.34}$$

where $\omega_+$ and $N_+$ are the parent statistical weights and populations densities of the parent system. The TE assumption enabled some degree of analysis to be performed on certain plasmas. For instance the fact that the sun's photosphere is approximately black body and emits a characteristic Planckian spectrum was used to determine that the photosphere has a temperature of $\sim 6,000K$.

Most plasmas have an escaping radiation field which acts to move the plasma away from conditions of TE. If all intrinsic and extrinsic time constants are much less that $\tau_{plasma}$ the collisions are efficient enough to overcome the population losses due to radiative decay, this is referred to as 'local thermodynamic equilibrium' (LTE). In

this case the TE equations hold for the free and bound particles, but the radiation field is that of a diluted black body. All systems will have a critical density above which collisions dominate over spontaneous emission losses. Spontaneous emission coefficients typically scale as $\sim 1/n'^5$ ($n'$ being the upper quantum shell), while electron collisional cross section scale as $\sim 1/n'^2$. Thus as one moves to higher quantum shells, LTE conditions becomes more valid.

If collisions are not able to compensate for radiation lossed the plasma is in 'non-local thermodynamic equilibrium' (NLTE). For most plasmas $\tau_{e-e} \ll \tau_o \ll \tau_m$ and for many plasma conditions (including fusion tokamaks) $\tau_{plasma} \sim \tau_{ion} \sim \tau_m$. In these conditions the free electrons have time to collisionally thermalise and form a Maxwellian velocity distribution. The excited states vary on a much quicker timescale that the metastables and can be considered to be in quasi-static equilibrium with them. The metastables thermalise on similar timescales to the plasma dynamics, as does the ionisation balance. So both the metastables and ionisation balance must be solved for dynamically within the context of plasma transport and ionisation balance codes. The excited state populations can then be evaluated with respect to the metastable populations. In solving for the excited state populations one must account for all the possible transitions between excited states as well as transitions to the metastables of the same and adjacent ionisation stages. This is referred to as the 'principle of statistical balance'. All the rates can be assembled into a system of equations describing the ways in which each atomic state can be populated and depoulated. This approach is referred to as the 'collisional-radiative' (C-R) approach, developed by Bates et al. (1962) and generalised by Summers & Hooper (1983) to account for metastables.

Consider an atomic energy level $i$ and assemble all the collisional, radiative and induced rates that can populate or depopulate it. The sum of all these rates equals the rate of change of the population density in that level. The general form of the statistical balance equations is as follows

$$\sum_{i'>i} \left[ A_{i'\to i} + \int_{line} u(\nu) B_{i'\to i} d\nu + N_e q^{(e)}_{i'\to i} + N_e q^{(p)}_{i'\to i} \right] N_{i'}$$

$$
\begin{aligned}
&+ \sum_{i''<i} \left[ \int_{line} u(\nu) B_{i''\to i} d\nu + N_e q^{(e)}_{i''\to i} + N_e q^{(p)}_{i''\to i} \right] N_{i''} \\
&+ N_e N_+ \alpha^{(r)}_i + N_e^2 N_+ \alpha^{(3)}_i + N_e N_+ \int u(\nu) B_{\kappa\to i} d\kappa \\
&= \left[ \sum_{i'>i} \left[ \int_{line} u(\nu) B_{i\to i'} d\nu + N_e q^{(e)}_{i\to i'} + N_e q^{(p)}_{i\to i'} \right] \right. \\
&+ \sum_{i''<i} \left[ A_{i\to i''} + \int_{line} u(\nu) B_{i\to i''} d\nu + N_e q^{(e)}_{i\to i''} + N_e q^{(p)}_{i\to i''} \right] \\
&+ \left. \int u(\nu) B_{i\to\kappa} d\kappa + N_e q^{(e)}_{i\to\varepsilon} + N_e q^{(p)}_{i\to\varepsilon} \right] N_i + \frac{dN_i}{dt}
\end{aligned}
\tag{1.35}
$$

Where .....

- $A_{i'\to i}$ - spontaneous emission from $i' \to i$
- $u(\nu) B_{i'\to i}$ - stimulated emission from $i' \to i$
- $u(\nu) B_{i\to i'}$ - photo-absorption from $i' \to i$
- $N_e q^{(e)}_{i'\to i}$ - electron collisonal de-excitation from $i' \to i$
- $N_e q^{(p)}_{i'\to i}$ - proton collisonal de-excitation from $i' \to i$
- $N_e q^{(e)}_{i\to i'}$ - electron collisional excitation from $i \to i'$
- $N_e q^{(p)}_{i\to i'}$ - proton collisional excitation from $i \to i'$
- $\int u(\nu) B_{i\to\kappa} d\kappa$ - photo-ionisation from $i$
- $N_e q^{(e)}_{i\to\varepsilon}$ - electron collisional ionisation from $i$
- $N_e q^{(p)}_{i\to\varepsilon}$ - proton collisional ionisation from $i$
- $N_e N_+ \alpha^{(r)}_i$ - radiative recombination to $i$
- $N_e^2 N_+ \alpha^{(3)}_i$ - three body recombination to $i$
- $N_e N_+ \int u(\nu) B_{\kappa\to i} d\kappa$ - stimulated recombination to $i$

A set of such equations can be assembled with one equation for each atomic energy level, $i$, that exists. It is the simultaneous solution of this set of equations that produces the atomic population structure. Because the excited state population values are in equilibrium with the metastable populations their $dN_i/dt$ terms can be set to zero.

One can write this set of equations in matrix notation indexed by i and j. Matrix elements such as $C_{ij}$ are made up from equation (1.35) and describe all the processes by which level $i$ can be populated from level j, written formally as

$$C_{ji} = A_{i\to j} + N_e q^{(e)}_{i\to j} + N_p q^{(p)}_{i\to j} + \ .... \tag{1.36}$$

The diagonal elements, such as $C_{ii}$, are the total loss rates from level $i$, given by

$$-C_{ii} = \sum_{j\neq i} C_{ji} + N_e q^{(e)}_{i\to\varepsilon} \tag{1.37}$$

Denoting metastable levels with greek subscripts, using the usual summation notation one has the following rate equation for level $\rho$ of ionisation stage $(z)$

$$\frac{dN^{(z)}_\rho}{dt} = C_{\rho\sigma}N^{(z)}_\sigma + C_{\rho j}N^{(z)}_j + C_{\rho\sigma_+}N^{(z+1)}_{\sigma_+} + C_{\rho\sigma_-}N^{(z-1)}_{\sigma_-} \tag{1.38}$$

and for excited state $i$ one has

$$0 = C_{i\sigma}N^{(z)}_\sigma + C_{ij}N^{(z)}_j + C_{i\sigma_+}N^{(z+1)}_{\sigma_+} + C_{i\sigma_-}N^{(z-1)}_{\sigma_-} \tag{1.39}$$

where $\sigma_-$ and $\sigma_+$ denote metastables of adjacent ionisation stages. The resulting set of equations are assembled into the collisional-radiative matrix and solved by matrix inversion for the excited state populations with respect to the metastables (which are assumed known from dynamical ionisation balance). For computational simplification the C-R matrix equation is conventionally solved using scaled temperatures and densities

$$t_e = \frac{kT_e}{I_H}\frac{1}{z_0^2} \tag{1.40}$$

$$t_r = \frac{kT_r}{I_H}\frac{1}{z_0^2} \tag{1.41}$$

$$\rho_e = 2^5\sqrt{\frac{\pi}{3}}\frac{\pi a_0^3}{\alpha^3}\frac{N_e}{z_0^7} \tag{1.42}$$

with similar definitions for the ion temperatures and densities. The population solution is expressed as deviation factors (referred to as 'b-factors') from Saha-Boltzmann values, defined via

$$N_i = N_+ N_e \left(\frac{h^2}{2\pi mkT}\right)^{\frac{3}{2}} \frac{\omega_i}{2\omega_+} e^{I_i/kT} b_i \tag{1.43}$$

Solving the equations for the b-factors provides a solution that is more easily interpreted (i.e. in 'LTE-space') and leads to cancellations which make the system numerically more stable. The equations can also be solved for c-factors ($= b - 1$), or $e^{I_i/kT_e} b_i$ factors. The choice of the 'picture' of the solution is determined by that which provides the most numerically stable solution. For example for very low $T_e$ the $b_i$ values can be very close to zero for the excited states and lead to numerical errors, whereas a solution in terms of $e^{I_i/kT_e} b_i$ is much more stable.

### Coupling schemes

In this work, a general population approach is developed which is valid for all ions, that is, of both light and heavy species in arbitrarily highly ionised systems. Thus energy level structures have to be dealt with which range from L-S terms (Russell-Saunders coupling) for light and near neutral systems to intermediate coupled levels for medium weight and fairly ionised systems ($z < 40$) to j-j coupled heavy, very highly ionised systems.

Although the existing light element coupling scheme, where a bundled-nS or bundled-nlSL electron sits on top of an L-S coupled core, provides the necessary precision for spectroscopic analysis of typical light element spectra, it encounters problems when extended to the sytems that are dealt with in this thesis. For heavy species the relativistic splitting of terms into fine structure levels becomes significant and the

resulting breakdown in L-S coupling, along with significant configuration interaction, means that the fine structure low lying level populations can no longer be assumed to be statistical and must be treated individually. This is reflected spectroscopically, where a J-resolved energy level picture is usually used for analysis of medium/heavy species. Also, the picture of a bundled-nS electron built on top of a metastable parent can no longer be sustained for highly excited populations. For such electrons, relativistic interaction dominates over electrostatic leading to spin system breakdown and it is more appropriate to model a weakly coupled nl electron built on a L-S coupled or intermediate coupling J core. This system is sometimes referred to as 'j-l coupled'. It should also be recognised that there is normally a change of the most appropriate coupling scheme as one passes from low levels to highly excited levels. Thus for the model presented in chapter 4 the following bundling regimes are defined, with each merging smoothly into the next as the levels become statistically populated and can be bundled over.

$$\begin{aligned} n < n_0 &: N_{(\gamma\pi J)} \\ n_0 < n \leq n_1 &: N_{(\gamma_p\pi_p J_p)nljJ} \\ n_1 < n \leq n_2 &: N_{(\gamma_p\pi_p J_p)nlj} \\ n_2 < n \leq n_3 &: N_{(\gamma_p\pi_p J_p)nl} \\ n_3 < n \leq n_4 &: N_{(\gamma_p\pi_p J_p)n} \end{aligned} \tag{1.44}$$

For $n < n_0$, the valence electron is in the core configuration and the multielectron states are in the form $\gamma\pi J$, where $\gamma$ is the configuration, $\pi$ the parity and $J$ the total angular momentum. For the rest of the bundling regimes one has an $nl$ electron built upon a J-coupled parent state $(\gamma_p\pi_p J_p)$ (henceforth referred to as the 'bundle-$(J_p)nl$' model). For $n_0 < n \leq n_1$ the J levels are treated individually, at $n_1$ they are effectively degenerate and statistically populated relative to each other and can be bundled together. Similarly at $n_2$ the j-states are effectively degenerate and statistically relatively populated and can be bundled over and at $n_3$ the l-states can be bundled over. Determining the point at which the collisional redistributive rates overcome the radiative decay rates allows the bundling cut-offs (i.e. $n_0 \rightarrow n_4$) to be evaluated. Work is presented in chapter 4 outlining a scheme by which these cut-offs can be detected automatically and used in the assembly of the appropriate collisional-radiative matrix - note that the increase in size of the working matrices necessary for this scheme is still within the capacity of modern workstations. The set of coupled models shown here marks a significant improvement over the existing scheme for light elements.

With the range of coupling schemes used in this new model it is necessary to define appropriate transformations between systems. Thus rates must be evaluated for cross-coupling transitions as well as for transitions within the new bundle-$(J_p)nl$ model. As most rate expressions contain their angular components within Gaunt factors, this leads to a need to derive Gaunt factors which deal with all the possible initial and final states of this new scheme. This has been done and the results summarised in table 4.1, with the details given in appendix A.

A progression of coupling schemes is used throughout this thesis. Chapters 1 and 2 examine opacity in light elements (C II in section 1.3.1 then generic light elements for the opacity work of chapter 2) using the existing ADAS light element coupling scheme. With the extension of the opacity work to high lying hydrogenic populations in chapters 3 and 5, a coupling scheme where an $nl$ electron sits on a bare nucleus is used. This leads on to the high level heavy species work of chapter 4 where the full bundle-$(J_p)nl$ model is used. Note that the code developed in chapter 4 is not the final heavy species one, but the hydrogenic module which will form the high quantum shell component of the final code. The concept of an excited hydrogenic electron coupled to a J-resolved core is a valid approximation for the highly excited states of heavy species, and provides a module that we can test against existing hydrogenic light element codes.

## 1.3 Examples of opacity and spectral series in astrophysical and laboratory plasmas

### 1.3.1 The solar atmosphere : branching line ratios as a diagnostic for deducing optical depth

Escape probabilities have often been used to diagnose optical depths (Jordan, 1967; Doyle & McWhirter, 1980; Keenan & Kingston, 1986; Kastner, 1999). As a demonstration of this technique consider an example taken from the study of Brooks et al. (2000). Observations were carried out on September 7th, 1996 using the SUMER (Wilhelm et al., 1995) instrument onboard the SOHO (SOlar and Heliospheric Observatory) spacecraft. The observations consisted of 18 cross-limb scans (in 1.9 arc sec steps) of the wavelength region surrounding various multiplets. We present the results for the C II $2s^2 2p\ ^2P$ - $2s2p^2\ ^2S$ (1036 Å) multiplet, see figure 1.8. The objective was to diagnose opacities from branching line ratio observations from the solar limb. This follows on from Doyle & McWhirter (1980) who performed a similar study on the C III $2s2p\ ^3P$ - $2p^2\ ^3P$ ($1175\mathring{A}$) multiplet.

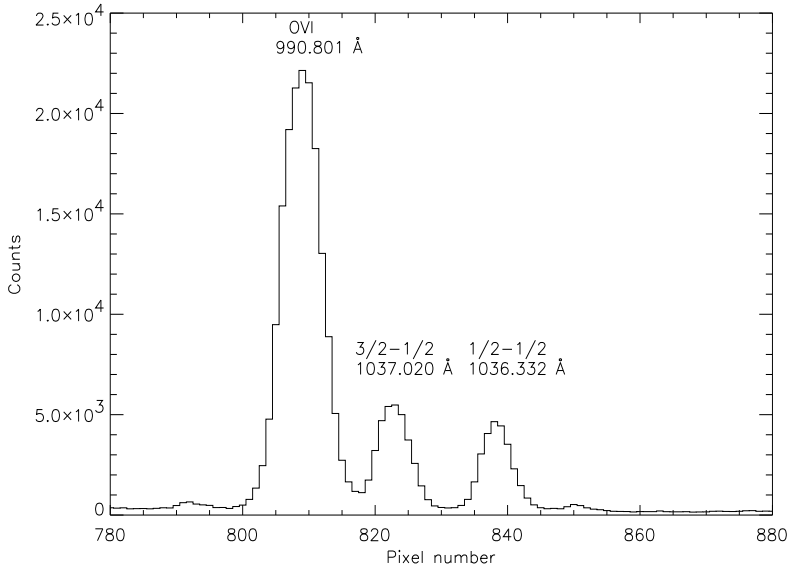


Figure 1.8: Spectrum of the CII multiplet used in the branching ratio study. The large line on the left hand side is a strong Oxygen line

In scanning across the limb of the sun, the geometrical thickness of the line of sight increases. Opacity effects in thick lines means that their fluxes will vary differently from those of the thin lines. The ratio of such lines allows the effects of opacity to be isolated.

Using equation (1.9) we see that the ratio of two spectral line intensities can be written as

$$\frac{I_{n_2' \to n_2}}{I_{n_1' \to n_1}} = \frac{\Theta_{n_2' \to n_2}}{\Theta_{n_1' \to n_1}} \frac{A_{n_2' \to n_2}}{A_{n_1' \to n_1}} \frac{\int_0^b N_{n_2'} dl}{\int_0^b N_{n_1'} dl} \tag{1.45}$$

where $n_1$ and $n_1'$ represent the lower and upper level indices respectively of line 1. Similarly $n_2$ and $n_2'$ represent the lower and upper level indices respectively of line 2. If the lines originate from the same upper level then $n_1' = n_2' = n'$ thus $N_{n_1'} = N_{n_2'} = N_{n'}$. That is,

$$\frac{I_{n_2' \to n_2}}{I_{n_1' \to n_1}} = \frac{\Theta_{n' \to n_2}}{\Theta_{n' \to n_1}} \frac{A_{n' \to n_2}}{A_{n' \to n_1}} \tag{1.46}$$

Thus observations of the ratio of two lines emitted from a common upper level,

C II $2s2p^2\ ^2S_{\frac{1}{2}}$ in our case, eliminates the dependence on the upper level population densities and isolates the opacity influence on the line ratio. Since the A-values are known, an observation of the intensity ratio leads to a deduced escape probability ratio, which in turn leads to an optical depth determination. The optical depth at line centre, taken from Mitchell & Zemansky (1961), is given by

$$\begin{aligned} \tau_0 &= \alpha(\nu_0)b \\ &= 1.16 \times 10^{-6}\sqrt{\frac{M}{T_i}}\lambda_0 f_{n'\to n} N_n b \end{aligned} \tag{1.47}$$

where
$T_i$ is the ion temperature [K].
$M$ is the atomic mass number of the absorbing atoms [a.m.u.].
$\nu_0$ is the central frequency of the transition of interest [Hz].
$\lambda_0$ is the central wavelength of the transition of interest [cm].
$N_n$ is the number density of the lower level of the transition [$cm^{-3}$].
$f_{n'\to n}$ is the absorption oscillator strength [dimensionless].
$b$ is the physical thickness of the plasma along the line of sight [cm].

Thus the ratio of two optical depths corresponding to lines which arise from the same upper level, $n'$, is given by

$$\frac{\tau_{0,n_1\to n'}}{\tau_{0,n_2\to n'}} = \frac{\lambda_{0,n_1\to n'}}{\lambda_{0,n_2\to n'}}\frac{f_{0,n_1\to n'}}{f_{0,n_2\to n'}}\frac{N_{n_1}}{N_{n_2}} \tag{1.48}$$

As the C II lines are close together, the ratio of the central wavelengths is close to unity and the $\tau$ ratio is controlled by the ratio of the two oscillator strengths and lower level populations, which are statistically populated. An optically thin population calculation using ADAS was done to verify this. It was found that the lower ground term relative populations were very close to statistical and insensitive to plasma conditions or finite optical depths. The following layer averaged escape probability expression (referred to as '$\bar{g}(\tau_0)$') was developed for an infinite plane parallel slab of homogeneous density

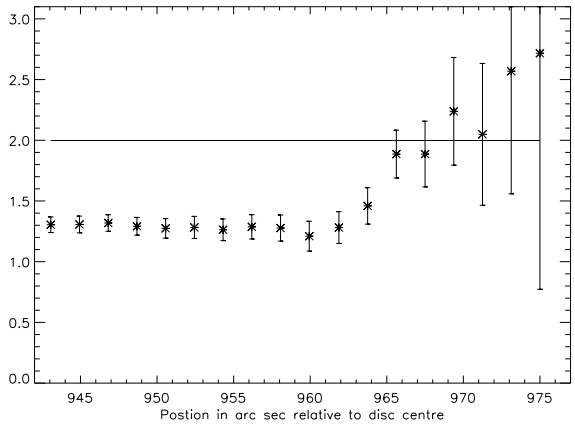


Figure 1.9: Plot of the C II $I(\frac{3}{2}-\frac{1}{2})/I(\frac{1}{2}-\frac{1}{2})$ line ratio . The solid line shows the optically thin flux ratio. The error bars reflect the uncertainty in the fitting of the two fluxes.

$$\bar{g}(\tau_0) = \frac{1}{\sqrt{\pi}} \int_{-\infty}^{\infty} \left[ \frac{1 - e^{-\alpha_0 \Delta x e^{-u^2}}}{\alpha_0 \Delta x} \right] du \tag{1.49}$$

Thus the method of analysis was as follows: Using equation (1.46) the ratio of the two escape probabilities was deduced from the intensity ratio observation. Then using expression (1.49) the corresponding optical depth ($\alpha_0 \Delta x$) in one of the transitions was evaluated numerically. Equation (1.48) was then used to deduce the optical depth in the other line and this was extrapolated to infer the optical depths of all other C II transitions.

In order to measure the line integrated spectral flux in each of the C II lines we used the fitting procedure ADAS 602 (Summers, 2001). This fitting routine performs a maximum likelihood fit of Gaussian profiles to an observed spectrum and produces integrated fluxes, central wavelength positions with associated error estimates. The resultant flux ratio plot is shown in figure 1.9 - note that the straight line in this figure shows the theoretical optically thin ratio, given by the ratio of the two A-values. The displayed errors are given by the square root of the sum of the squares in the errors in the fluxes for each line.

The ratio $I(\frac{3}{2}-\frac{1}{2})/I(\frac{1}{2}-\frac{1}{2})$ deviates significantly from its optically thin value on disc and at the limb ($\approx$ 959 arc sec), returning to its thin value above the limb. Neither

| Pos.(") | $\bar{g}_{3/2-1/2}$ | $\tau_{0,3/2-1/2}$ | Pos.(") | $\bar{g}_{3/2-1/2}$ | $\tau_{0,3/2-1/2}$ |
|---|---|---|---|---|---|
| 943.06 | 0.31 | 5.30 | 959.94 | 0.18 | 10.2 |
| 944.94 | 0.31 | 5.25 | 961.88 | 0.28 | 6.00 |
| 946.81 | 0.32 | 4.95 | 963.75 | 0.46 | 2.82 |
| 948.69 | 0.29 | 5.70 | 965.63 | 0.88 | 0.36 |
| 950.56 | 0.27 | 6.23 | 967.50 | 0.88 | 0.36 |
| 952.44 | 0.28 | 6.00 | 969.38 | - | - |
| 954.31 | 0.26 | 6.70 | 971.25 | - | - |
| 956.19 | 0.29 | 5.80 | 973.13 | - | - |
| 958.06 | 0.27 | 6.20 | 975.00 | - | - |

Table 1.1: Summary of the data for the C II $2s^2 2p\ ^2P_{3/2} - 2s2p^2\ ^2S_{1/2}$ transition for each raster scan position.

line shows much limb brightening, indicating that they are both optically thick on disc. The $(3/2 - 1/2)$ line is expected to be more sensitive to changes in opacity as it has a greater oscillator strength and statistical weight and therefore an increased optical depth. On disc and at the limb this line experiences a bigger reduction in intensity and the intensity ratio is lower than its optically thin value. Above the limb the density of the plasma falls off and the fluxes (and hence the line ratios) should return to their optically thin values. This appears to be the case here, but further study indicates that scattered light, or unresolved fine structures beyond the limb, modifies this simple conclusion (Fischbacher, 2001). Using the method described above the optical depths in the $(3/2 - 1/2)$ line were evaluated at each scan position and are shown in table 1.1. In Brooks et al. (2000) the optical depths are extrapolated to classify the transitions in different C II lines and a similar study is also performed on other carbon multiplets.

This technique of determining the optical depths in all the lines of one ion from a single branching line ratio has provided us with a powerful characterisation of lines which are optically thin, and hence suitable for Differential Emission Measure (DEM) analysis. Alternatively, escape probabilities can be used to adjust observed intensities of optically thick lines, allowing them to be used in such a study. Thus it is possible

to diagnose optical depths in a moderately optically thick plasma from branching line ratio observations using escape probability techniques.

### 1.3.2 Low hydrogen series member opacity : Fusion divertor plasma

Consider next the case of hydrogen opacity in the fusion tokamak divertor region. The divertor (see figure 1.10) is situated below a null point in the tokamak poloidal magnetic field such that plasma impurities entering the scrape-off layer flow unimpeded to the target plates and are filtered out from the main body of the plasma. The plasma impurities and spent fuel experience collisions and possibly radiative cooling upon entry into the divertor reducing their energies and momenta. Thus when they encounter the divertor target plate strike points they are less effective in sputtering material back into the plasma core. The reverse flow in the divertor assists in constraining any ejected material and returning it towards the divertor, allowing it to be extracted by the cryopump. The divertor region is a low temperature ($\approx 1 \times 10^4 K$), high density ($\approx 1 \times 10^{13} cm^{-3}$) plasma where the electrons and ions may recombine and a high concentration of neutrals are present. The neutral presence is maintained by the recycling of hydrogen on the walls and by direct gas puffing into the divertor. Under these conditions and effective plasma dimensions, one might expect the lowest hydrogen Lyman lines to become optically thick, although the Balmer lines would certainly remain thin. Opacity in the $L_\beta$ line has been observed in ASDEX-upgrade (Behringer, 1997) and in the JET divertor (Lachin, 1997). In JET it was found that there was significant line absorption in $L_\alpha$ but that it did not affect the ionisation balance or power loss. Wan et al (1995) used an escape factor approach to predict the effects of $L_\alpha$ absorption in projected ITER conditions, finding that opacity will have to be included in ionisation balance and power loss calculations.

The optically thin branching line ratio of $L_\beta/H_\alpha$ from equation (1.46) is 0.79. Observations taken from Behringer (1998) on the ASDEX-upgrade measured it to be about 4.0, indicating $L_\beta$ opacity. An escape probability and absorption factor code has been developed by Behringer and translated into the ADAS code, ADAS 214. See

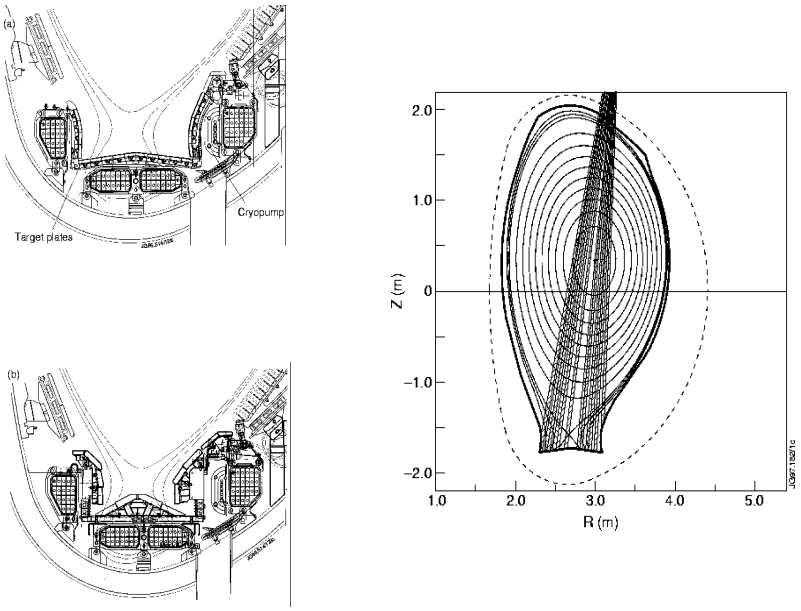


Figure 1.10: Schematic of JET tokamak divertor region showing the target plates and cryopump.

the code and theory description as given in Behringer (1998) and the description in chapter 2. The following example is taken from the Behringer's report and provides a useful illustration of the generic (i.e. scalable) application of absorption factors to account for opacity modifications to atomic population structure. The code was run for hydrogen emission in the divertor region with the following options: a voigt line profile was chosen with the Lorentz half width being 0.14 times the doppler half width (see Behringer (1998) for justification of this choice). A gas temperature of 23,010 K and an electron temperature of 11,605 K were selected. A cylindrical plasma geometry was chosen with an aspect ratio of 5. The effective length of the plasma was chosen to be 7.5 cm and the column density (=length $\times$ plasma density) varied from $2 \times 10^{14}$ $cm^{-2}$ to $1.2 \times 10^{15}$ $cm^{-2}$. A parabolic decrease in the upper level density distribution was selected and the line ratios predicted. The results of the code are shown in figures 1.11 and 1.12.

In figure 1.11 the absorption factors evaluated at a column density of $1 \times 10^{14}$ $cm^{-2}$ are shown. The y-axis gives the absorption factor value while the x-axis shows the optical depth calculated for the various transitions. Note that the absorption factor

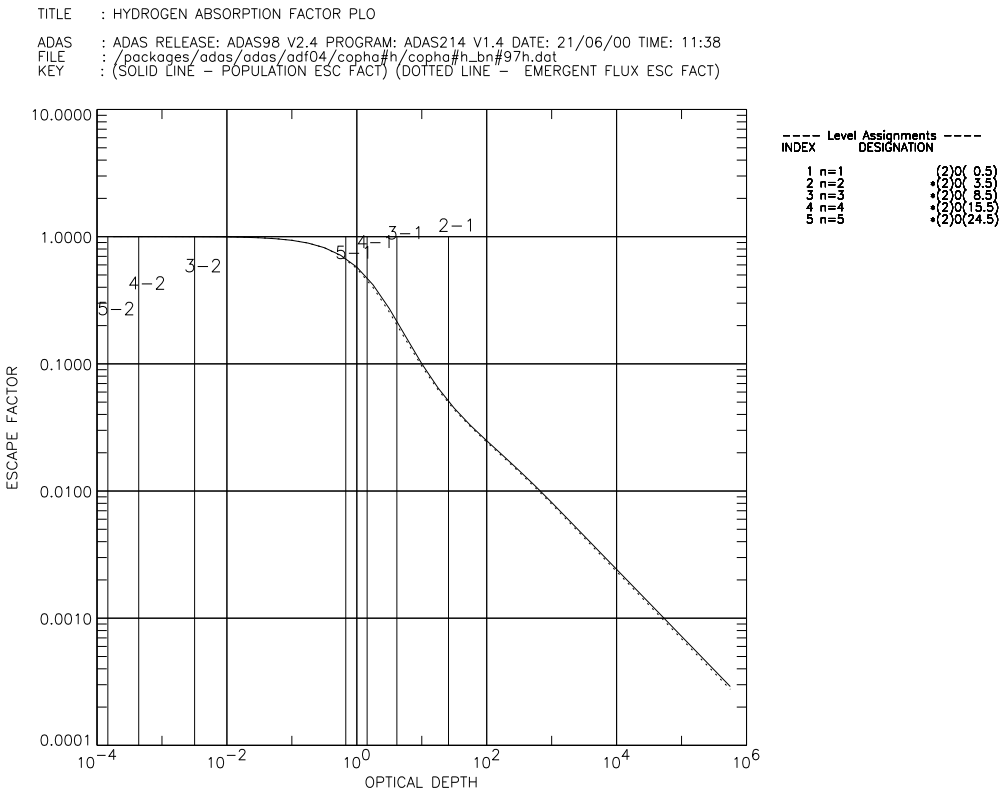


Figure 1.11: Absorption factor results for hydrogen from Behringer (1998) reproduced using ADAS 214. The index numbers labelling the vertical lines correspond to the principal quantum shell of the upper and lower states.

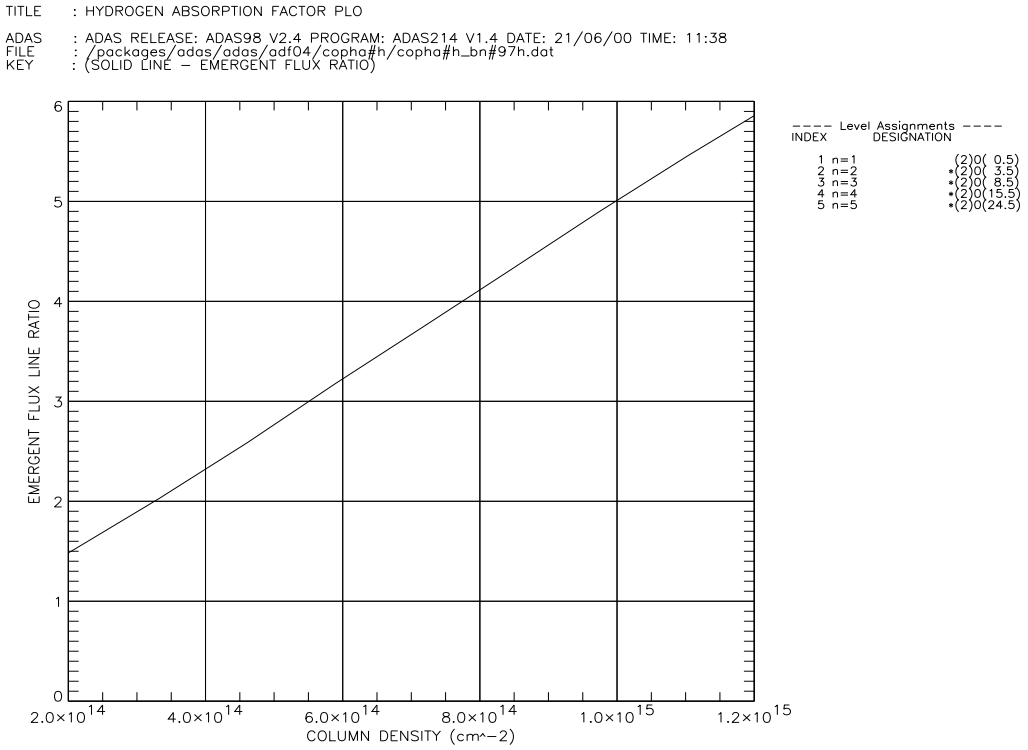


Figure 1.12: Opacity modified line ratio results from ADAS 214 for divertor conditions.

curve is represented by the solid line and the escape probability curve by the dotted line. A vertical line is drawn for the first few Lyman and Balmer transitions, and where these lines cut the absorption factor curve one can read off the absorption factor for that transition. All the Balmer lines have negligible absorption factors and escape probabilities, while the Lyman lines are moderately thick.

Figure 1.12 shows the predicted intensity line ratio of $L_\beta/H_\alpha$ as a function of column density. Optically thick population densities are used in this calculation by modifying the spontaneous emission coefficients in the collisional-radiative subroutine of ADAS 214 by the appropriate absorption factors. The escaping flux for each line is then modified by that line's escape probability and the optically thick line ratio found. It can be seen that the column density corresponding to the observed $L_\beta/H_\alpha$ line ratio of 4.0 is approximately $7.5 \times 10^{14}\ cm^{-2}$, which implies a neutral hydrogen density of $1.0 \times 10^{14}\ cm^{-3}$, broadly consistent with divertor conditions.

Using absorption factor techniques such as the one outlined here, opacity adjustments to moderately optically thick plasma population densities can be found.

### 1.3.3 High hydrogen series member opacity: Solar prominence Lyman lines, Lyman continuum and Balmer line radiation

Spectral observations of solar prominences show that they are optically thick in all Lyman lines through to the Lyman continuum. Figure 1.13 gives an $H\alpha$ image of a prominence and figure 1.14 an example of an optically thick Lyman series limit spectrum.

Solar prominences are large, dense, cool structures in the solar atmosphere, immersed in a background radiation field from the solar photosphere and chromosphere. Reviews can be found in Hirayama (1985), Zirker (1988), Preist (1989) and Tandberg-Hanssen (1995). See table 1.2 for typical physical values. They are stable on a timescale of weeks until they often erupt from the solar atmosphere. They are sometimes associated with Coronal Mass Ejections (CME's), though the nature of the association is unclear. There is much interest in solar prominences at the moment,

Figure 1.13: Solar prominence $H\alpha$ observation taken by the janitor of the Big Bear Solar observatory in 1970. Note the various characteristic prominence components, i.e. a large body of plasma suspended in the corona with a few footpoints rooted in the photosphere. On close inspection the vertical fillamentary internal structure of the prominence can be seen.

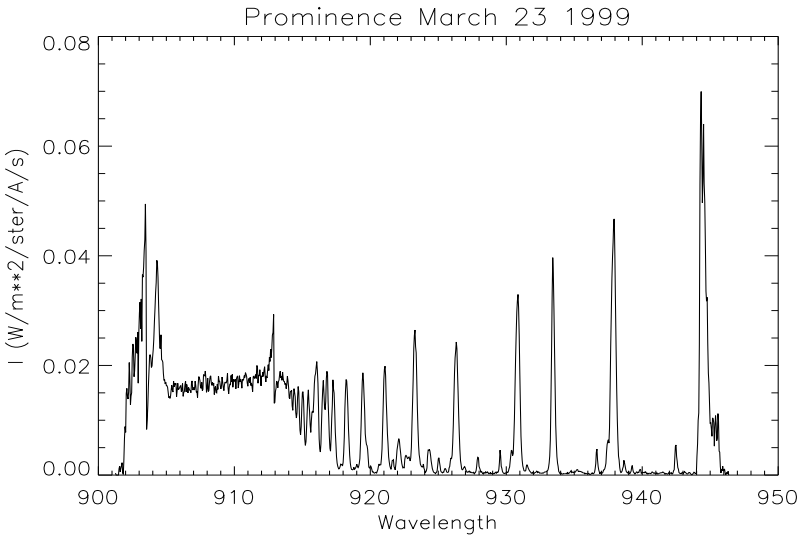


Figure 1.14: Lyman series limit observation of a solar prominence, taken from the data in Schmieder et al. (1999b). Note the merging of the high series lines into the continuum. Compare the heights of the last few observable lines with the gain in line heights as one progresses down the series. The small increase indicates that the lines are not reflecting optically thin conditions with Boltzmann upper level densities, but are being significantly reabsorbed.

| Quantity | typical values |
|---|---|
| Electron density | $5 \times 10^{10} - 1 \times 10^{11} cm^{-3}$ |
| Electron pressure | $0.1\ dyn\ cm^{-2}$ |
| Temperature | $7,000K$ |
| Gas pressure | $3 - 6\ dyn\ cm^{-2}$ |
| Hydrogen density | $3 \times 10^{11}\ cm^{-3}$ |
| Size | $100,000 - 600,000km$ long<br>$5,000 - 10,000km$ thick<br>$50,000km$ high |
| Ionisation degree of hydrogen | 0.07 |

Table 1.2: Summary table of typical prominence physical properties.

in particular in explaining their support mechanism in the solar atmosphere and the trigger for their abrupt eruption, see Schmieder et al. (1998), Schmieder et al. (1999a), Schmieder et al. (1999b), Schmieder et al. (2000), Stellmacher & Wiehr (1994).

The optical thickness of the Lyman series is easily seen from an estimate of photon mean free paths (given by the reciprocal of the absorption coefficient), compare the mean free paths of table 1.3 with typical prominence dimensions. The Lyman series photons are heavily absorbed, with a mean free path of less than a centimeter, while the Balmer series photons have mean free paths of the same order as the dimension of the prominence. A consequence of this heavy absorption is the unusual energy balance for prominences, first found by Poland and Anzer (1971). It is likely that the main energy gain is due to Lyman continuum absorption, and that the main losses are due to H$\alpha$ emission. Photo-absorption of Lyman lines is the dominant process in populating the excited states of the prominence hydrogen atoms. Similarly absorption of the Lyman continuum drives the ionisation balance of both hydrogen and helium atoms in the plasma.

The presence of opacity in all Lyman lines through to and including the continuum led to the development of the analytically continuous escape probability and absorption factor expressions shown in chapter 3. These expressions allow opacity to be dealt with as series limit lines merge together and blend into the continuum, thus providing

| Transition | mean free path (m) |
|---|---|
| 2-1 | $1.41 \times 10^{-2} m$ |
| 3-1 | $8.82 \times 10^{-2} m$ |
| 4-1 | $0.25 \times 10^{0} m$ |
| 5-1 | $0.54 \times 10^{0} m$ |
| 3-2 | $9.42 \times 10^{4} m$ |
| 4-2 | $6.84 \times 10^{5} m$ |
| 5-2 | $2.04 \times 10^{6} m$ |
| 4-3 | $2.56 \times 10^{5} m$ |
| 5-3 | $2.09 \times 10^{6} m$ |
| 5-4 | $1.62 \times 10^{5} m$ |

Table 1.3: Summary table of typical mean free paths of hydrogen photons in a solar prominence.

a means of analysing spectra such as the one shown in figure 1.14. However, the large optical depths of prominences puts them into a regime where a radiative transfer approach is more appropriate. There already exist low series member prominence radiative transfer codes (Heasley & Mihalas, 1976 and Gouttebroze et al., 1993). It has been demonstrated that a radiative transfer approach which allows for partial frequency redistribution (PRD) is necessary to match the observed low series member line profiles and to properly account for population modification (Gouttebroze et al., 1993). It may be possible to construct a valid high series escape factor code, as the higher populations will be close to Boltzmann values so the coupling of the equations (1.1) and (1.35) is not an issue. Also, partial frequency redistribution, which must be accounted for in the low series members, becomes less significant as one progresses up a series and complete frequency redistribution (CRD) can be assumed. It was decided that no diagnostic advantage would be achieved from developing such a code and that the code of chapter 3 should be retained for plasmas with more moderate optical depths.

The prominence observations raise one final issue. That is, there are plasmas for which the influence of a background radiation field on our escape and absorption factor expressions should be included. Normally the background radiation field term

in equation (1.8) and the background radiation field contribution to $u(\nu)$ in equation (1.14) are set to zero. It proves fairly straightforward to include such a background field in the theory development for the escape probability and absorption factor expressions. This was done and the initial steps in developing a corresponding code were performed, see section 2.10.

### 1.3.4 High series observations : Fusion divertor plasma

Although series limit prominence observations could not be modelled, there existed a need to interpret similar fusion divertor spectra. These types of series limit spectra were first analysed by Inglis & Teller (1939), where the smooth merging of high series lines into the continuum was shown and the point at which the merging occurred used as a density diagnostic. Recently more advanced models have been developed allowing series limits to be included in solar atmosphere codes (Dappen, et al., 1987), in atomic calculations for the IRON project (Seaton, 1990) and to interpret tokamak divertor spectra (Pigarov et al., 1998). Figure 1.15 shows an example of a Balmer series limit observed on the JET reactor, taken from Meigs et al. (1998).

As one progresses up a series, the spectral lines blend together and assignment of a photon to a particular upper level becomes ambiguous. The merged lines smoothly extend into the continuum, and it becomes difficult to define a sharp continuum edge. This adds uncertainty to electron temperature and density diagnostics which depend upon the continuum edge (such as those described in chapters 10 and 11 of Griem (1997)). A code was developed to predict a synthetic spectrum, referred to as a 'spectral feature', of sufficient quality that the fitting of this feature to JET divertor spectra could be used to diagnose plasma electron temperature, density and recombination state.

Comprehensive modelling of this region requires high quality line profiles for the high series members, the population modelling must be appropriate for high quantum shells and the smooth merging of high series lines into the continuum has to be accounted for. The conventional method of dealing with the series merging is to introduce a statistical microfield which progressively shifts the high quantum shells into the

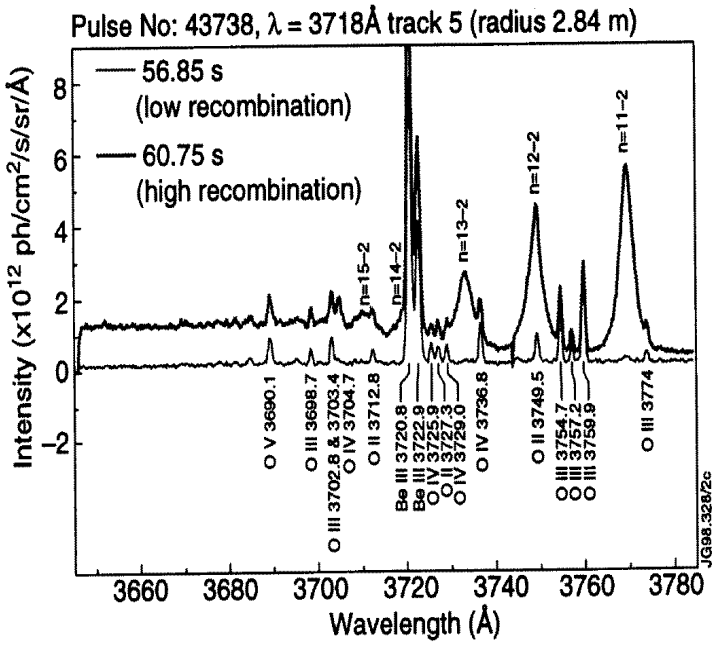


Figure 1.15: Balmer series limit observation of the JET divertor region, taken from Meigs et al. (1998).

continuum through field ionisation. That is, it is assumed that once an electron reaches a certain n-shell it is automatically ionised and thus behaves as if it is in the continuum. See Pigarov et al. (1998) for an example of this method used in practice to deal with series merging in the divertor of the Alcator C-Mod tokamak. This thesis takes an alternative approach, proving that bound-bound photo-rates continue analytically into the free states, with no need to 'dissolve' high quantum shells into the continuum. The microfield effects are accounted for in the line broadening calculations and it is intended that they will be included (as an extra rate, not as an ionising field) in future collisional-radiative work . The details of this alternative approach are presented in chapter 3 and a contrast with the conventional method given in section 3.3. It will be shown in section 5.3.3 that the JET divertor code can indeed fit observational data and diagnose local plasma parameters.